Am J Physiol Lung Cell Mol Physiol 298: L45–L56, 2010.
First published November 6, 2009; doi:10.1152/ajplung.90550.2008.

Lunatic Fringe-mediated Notch signaling is required for lung alveogenesis

Keli Xu,[1] Erica Nieuwenhuis,[1] Brenda L. Cohen,[1] Wei Wang,[1] Angelo J. Canty,[2] Jayne S. Danska,[3] Leigh Coultas,[1] Janet Rossant,[1,4] Megan Y. J. Wu,[1] Tino D. Piscione,[1] Andras Nagy,[4,5] Achim Gossler,[6] Geoff G. Hicks,[7] Chi-Chung Hui,[1,4] R. Mark Henkelman,[8] Lisa X. Yu,[8] John G. Sled,[8] Thomas Gridley,[9] and Sean E. Egan[1,4]

[1]*Program in Developmental and Stem Cell Biology, The Hospital for Sick Children, Toronto;* [2]*Department of Mathematics and Statistics, McMaster University, Hamilton; and* [3]*Program in Genetics and Genome Biology, The Hospital for Sick Children, and Department of Immunology and Department of Medical Biophysics, Institute of Medical Sciences, University of Toronto,* [4]*Department of Molecular Genetics, University of Toronto, and* [5]*Samuel Lunenfeld Research Institute, Mount Sinai Hospital, Toronto, Ontario, Canada;* [6]*Institute for Molecular Biology, Medizinische Hochschule Hannover, Hanover, Germany;* [7]*Manitoba Institute of Cell Biology, Winnipeg, Manitoba, Canada;* [8]*Mouse Imaging Centre, Hospital for Sick Children and University of Toronto, Toronto, Ontario, Canada; and* [9]*The Jackson Laboratory, Bar Harbor, Maine*

Submitted 6 November 2008; accepted in final form 12 October 2009

Xu K, Nieuwenhuis E, Cohen BL, Wang W, Canty AJ, Danska JS, Coultas L, Rossant J, Wu MY, Piscione TD, Nagy A, Gossler A, Hicks GG, Hui CC, Henkelman RM, Yu LX, Sled JG, Gridley T, Egan SE. Lunatic Fringe-mediated Notch signaling is required for lung alveogenesis. *Am J Physiol Lung Cell Mol Physiol* 298: L45–L56, 2010. First published November 6, 2009; doi:10.1152/ajplung.90550.2008.—Distal lung development occurs through coordinated induction of myofibroblasts, epithelial cells, and capillaries. *Lunatic Fringe* (*Lfng*) is a β_{1-3} *N*-acetylglucosamine transferase that modifies Notch receptors to facilitate their activation by Delta-like (Dll1/4) ligands. Lfng is expressed in the distal lung during saccular development, and deletion of this gene impairs myofibroblast differentiation and alveogenesis in this context. A similar defect was observed in *Notch2*$^{\beta\text{-}geo/+}$*Notch3*$^{\beta\text{-}geo/\beta\text{-}geo}$ compound mutant mice but not in *Notch2*$^{\beta\text{-}geo/+}$ or *Notch3*$^{\beta\text{-}geo/\beta\text{-}geo}$ single mutants. Finally, to directly test for the role of Notch signaling in myofibroblast differentiation in vivo, we used *ROSA26*-rtTA$^{/+}$;tetO-*CRE*$^{/+}$;*RBPJ*$\kappa^{flox/flox}$ inducible mutant mice to show that disruption of canonical Notch signaling during late embryonic development prevents induction of smooth muscle actin in mesenchymal cells of the distal lung. In sum, these results demonstrate that *Lfng* functions to enhance Notch signaling in myofibroblast precursor cells and thereby to coordinate differentiation and mobilization of myofibroblasts required for alveolar septation.

alveolar development

LUNG DEVELOPMENT IS A COMPLEX process requiring coordinated interaction between epithelial and mesenchymal cell types. Ultimately, lung parenchyma is subdivided to create a structure with extremely high surface-to-volume ratio, made up of millions of alveoli. During alveogenesis, a multilayered wall of cells is transformed into a thin epithelial/capillary wall containing type II and type I cells, involved in surfactant secretion and gas exchange, respectively, as well as microcapillaries, fibroblasts, and elastic extracellular matrix (4, 44). Myofibroblast differentiation and mobilization within this preexisting multilayered wall is a critical step in alveolar formation (27, 44).

Notch receptors are large EGF-repeat-containing transmembrane proteins, with cytoplasmic domains that bind to a DNA-binding protein, RBPJκ/CSL. Mammals have four Notch receptor genes (Notch1, 2, 3, and 4). A canonical Notch pathway is activated when a ligand, expressed on the surface of one cell, activates Notch on the surface of a neighboring cell (14, 29). Once activated, Notch is cleaved in a two-step process involving the γ-secretase complex. This cleavage releases a cytoplasmic domain fragment (Notch^{IC} or N^{IC}) that translocates into the nucleus, where it binds to an RBPJκ-containing complex, converting it from a transcriptional repressor into an activator. Thus activated N^{IC} induces expression of genes that had been repressed by RBPJκ in the absence of Notch signaling. Notch receptor signaling is activated by Delta/Dll or Serrate/Jagged family ligands. Interestingly, a *N*-acetylglucosamine sugar transferase, Fringe, was identified in *Drosophila* that controls which of these two ligand types activate Notch in many developmental contexts (20). Mammals have three Fringe genes: *Lunatic Fringe* (*Lfng*), *Manic Fringe* (*Mfng*), and *Radical Fringe* (*Rfng*) (5, 24). Genetic studies have identified a large number of tissues where Dll-Notch or Jagged-Notch signaling plays a critical role, and indeed fringe genes are expressed in many of these (5, 24). Despite this, very little is known about how fringes control Notch-dependent development. During somitogenesis, *Lfng* regulates the molecular clock by restricting Notch activation downstream of Dll ligands (13, 18, 47, 56). Similarly, *Lfng* facilitates Notch activation by Dll-family ligands during lymphocyte, blood vessel, and neuronal development (2, 37, 49, 50, 55).

Multiple Notch ligands and receptors are expressed in the developing lung (28, 42), and expression of most of these rise dramatically as lung parenchyma and vascular development proceed (48). A number of elegant studies have highlighted the importance of Mash1 and Hes1, Notch-regulated transcription factors, in specification of neuroendocrine cells of the neuroepithelial body (NEB) and neighboring Clara cells (6, 23). Notch signaling has also been shown to induce secretory cell fate in the proximal lung and can suppress specification and/or differentiation of alveolar epithelial cell types when ectopically activated (7, 19, 52, 53).

Although Notch signaling has been shown to regulate development of lung epithelium and endothelium, it is not yet clear whether it controls development of pulmonary mesenchymal cell types such as myofibroblast cells, which are required for septation of developing alveoli (43). Several in vitro studies have suggested that Notch signaling may indeed regulate myofibroblast specification and/or differentiation. For

Address for reprint requests and other correspondence: S. E. Egan, Program in Developmental and Stem Cell Biology, The Hospital for Sick Children, 101 College St., East Tower, Rm. 14-309, Toronto, Ontario, Canada M5G 1L7 (e-mail: segan@sickkids.ca).

example, transforming growth factor-β (TGF-β)-induced differentiation of C2C12 cells into myofibroblasts was inhibited by Notch2 but enhanced by Notch3 (39), whereas TGF-β-induced differentiation of 10T1/2 cells into myofibroblasts was blocked by Notch3 (25). In addition, Fizz1/Relmα-induced differentiation of adult lung fibroblasts into myofibroblasts was dependent on Notch1 (32). Thus the effect of Notch on myofibroblast differentiation can be either stimulatory or inhibitory, depending on the cell of origin, the inducer, and the specific Notch-receptor involved. In each case, however, the effect of canonical Notch signaling on myofibroblast gene expression is most likely direct. For example, smooth muscle actin-α (sma) expression can be induced through binding of a $Notch^{IC}$-RBPJκ complex to the sma promoter or repressed though binding of Hes/Hey complexes to a distinct *cis*-element (9, 34, 38, 39, 45). Here, we report that *Lfng* functions to enhance Notch-dependent induction of myofibroblast differentiation during embryonic lung development in the mouse.

MATERIALS AND METHODS

Targeting strategy and generation of mice. Lfng was targeted in 129 embryonic stem (ES) cells using a vector containing 3 loxP sites and a Pgk-*neo* cassette flanked by loxP and Flippase recognition target (FRT) sites. Two targeted clones were used to generate germline chimeric mice following injection into C57BL/6 blastocysts, and 2 independent germline transmission lines of $Lfng^{neo/+}$ were established. The $Lfng^{flox}$ allele was generated by crossing $Lfng^{neo/+}$ with *Rosa26-Flp* mice (Stock Number 003946, The Jackson Laboratory; K. Xu and S. E. Egan, unpublished observations). The $Lfng^{\Delta 2}$ allele, hereafter referred to as $Lfng^{-}$, was generated by crossing $Lfng^{flox/+}$ with *EIIa-Cre* mice (Stock Number 003724, The Jackson Laboratory; Ref. 30). Generation of $Lfng^{lacZ}$ mice was previously described (56). $Lfng^{\Delta 2/\Delta 2}$ and $Lfng^{lacZ/lacZ}$ mutant mice exhibit similar defects in somite patterning as well as alveolar development in the lung. Also, we have observed a slightly, but significantly, lower than expected number of homozygous mutant mice born with both alleles. The reason for this has not been explored. Abnormal lung development is most severe when these mutations were backcrossed to the FVB mouse strain, with 100% penetrance in both sexes. Therefore, all phenotypic analyses of *Lfng* mutants ($Lfng^{\Delta 2/\Delta 2}$ and $Lfng^{lacZ/lacZ}$) were conducted after backcrossing to FVB for at least 6 generations. $Jagged1^{\beta\text{-}geo/+}$, $Notch2^{\beta\text{-}geo/+}$, and $Notch3^{\beta\text{-}geo/+}$ mutant mice were generated using ES cell lines obtained from BayGenomics (gene trap lines KST248, LST103, and PST033, respectively). All experiments were performed according to guidelines from the Canadian Council on Animal Care and were approved by the Animal Care Review Committee at the Hospital for Sick Children. Finally, mice were housed in standard microisolator cages.

Temporal deletion of RBPJκ in vivo. A tetracycline-inducible (Tet-On) transgenic system was used to induce ubiquitous Cre-loxP-dependent temporal gene inactivation in *RBPJκ* conditional null ($RBPJ\kappa^{flox}$) mouse embryos. This system employs two transgenic mouse lines, *ROSA26*-$rtTA^{neo\text{-}out}$ and *tetO*-CRE, which, when crossed together and treated with systemic administration of the tetracycline analog doxycycline (DOX), generate progeny that express Cre recombinase (CRE) in a wide range of cell types (1). *ROSA26*-$rtTA^{neo\text{-}out}$

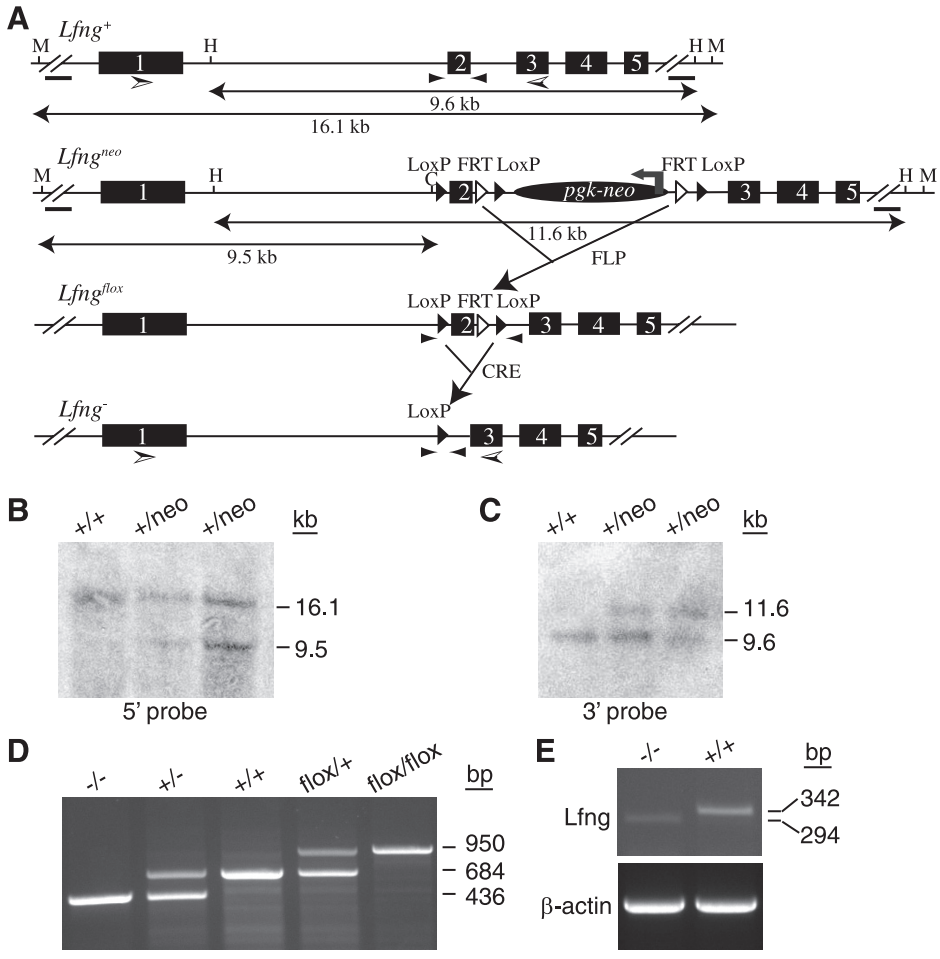

Fig. 1. Generation of *Lunatic Fringe* (*Lfng*) mutant mice. *A*: generation of *Lfng* mutant alleles. The $Lfng^{+}$ wild-type allele is shown at the *top* with numbered boxes representing exons. The $Lfng^{neo}$ allele contains 3 loxP sites and 2 Flippase recognition target (FRT) sites, a Pgk-*neo* cassette flanked by loxP and FRT sites. The $Lfng^{flox}$ allele, with exon 2 floxed, was generated by crossing $Lfng^{neo/+}$ with *Rosa-Flp* mice. The $Lfng^{-}$ allele, with exon 2 deleted, was generated by crossing $Lfng^{flox/+}$ with *EIIa-Cre* mice. The bars represent 5′ and 3′ probes for Southern blot analysis. Small and large arrowheads indicate primers for PCR genotyping and RT-PCR, respectively. *B*: Southern blot analysis of targeted embryonic stem (ES) cell genomic DNA digested with MPh1103I (M) and *Cla*I (C) using 5′ probe. *C*: Southern blot analysis of targeted ES cell genomic DNA digested with *Hin*dIII (H) using 3′ probe. *D*: a representative gel of PCR genotyping for Lfng mutant mice. *E*: RT-PCR on total RNA from $Lfng^{-/-}$ and wild-type lungs. Note the $Lfng^{-/-}$ mutant lung expressed reduced level of a truncated transcript. CRE, Cre recombinase.

(hereafter referred to as *ROSA26-rtTA*) was generated by crossing *ROSA26-rtTA*, *EGFP (neo-in)* (1) to a universal Cre deleter line (pCX-nls-Cre; Ref. 35) to remove stop transcription sequences and thereby generate a line expressing rtTA in every tissue. *tetO*-CRE and *RBPJκ*$^{flox/flox}$ mouse lines have been previously described (21, 41, 51). A multistage breeding strategy was employed to ultimately generate *ROSA26*-rtTA$^{/+}$; *tetO*-CRE$^{/+}$; *RBPJκ*$^{flox/flox}$ compound mutant embryos. Mouse genotyping was performed by PCR as previously described (1, 21, 41, 51). To induce temporal deletion of *RBPJκ* in mouse embryos, DOX was administered ad libitum to pregnant *RBPJκ*$^{flox/flox}$ females (bred with *ROSA26*-rtTA$^{/+}$; *tetO*-CRE$^{/+}$;RBPJκ$^{flox/+}$ male) by adding drug (2 mg/ml doxycycline hyclate in 5% sucrose; Sigma, St. Louis, MO) to their drinking water starting at pregnancy *day 14.5*; this yields effective DOX uptake by embryos via placental transfer (1). At *day 18.5* of gestation (18.5 dpc), pregnant mice were euthanized, embryos harvested, and tissues procured by microdissection. The majority of DOX-exposed *ROSA26*-rtTA$^{/+}$;tetO-*CRE*$^{/+}$; *RBPJκ*$^{flox/flox}$ compound mutant pups die shortly after birth. A few such mutants were euthanized at postnatal *day 0* (P0) for analysis of neonatal lung development.

Primers and probes. The targeted ES clones were confirmed by Southern blot analysis using a PCR-cloned 749-bp fragment mapping 2.4 kb upstream of the start codon (5′ probe) and a PCR-cloned 643-bp fragment from 1.6 kb downstream of the stop codon (3′ probe). The genotype of *Lfng* mutant mice was established by PCR

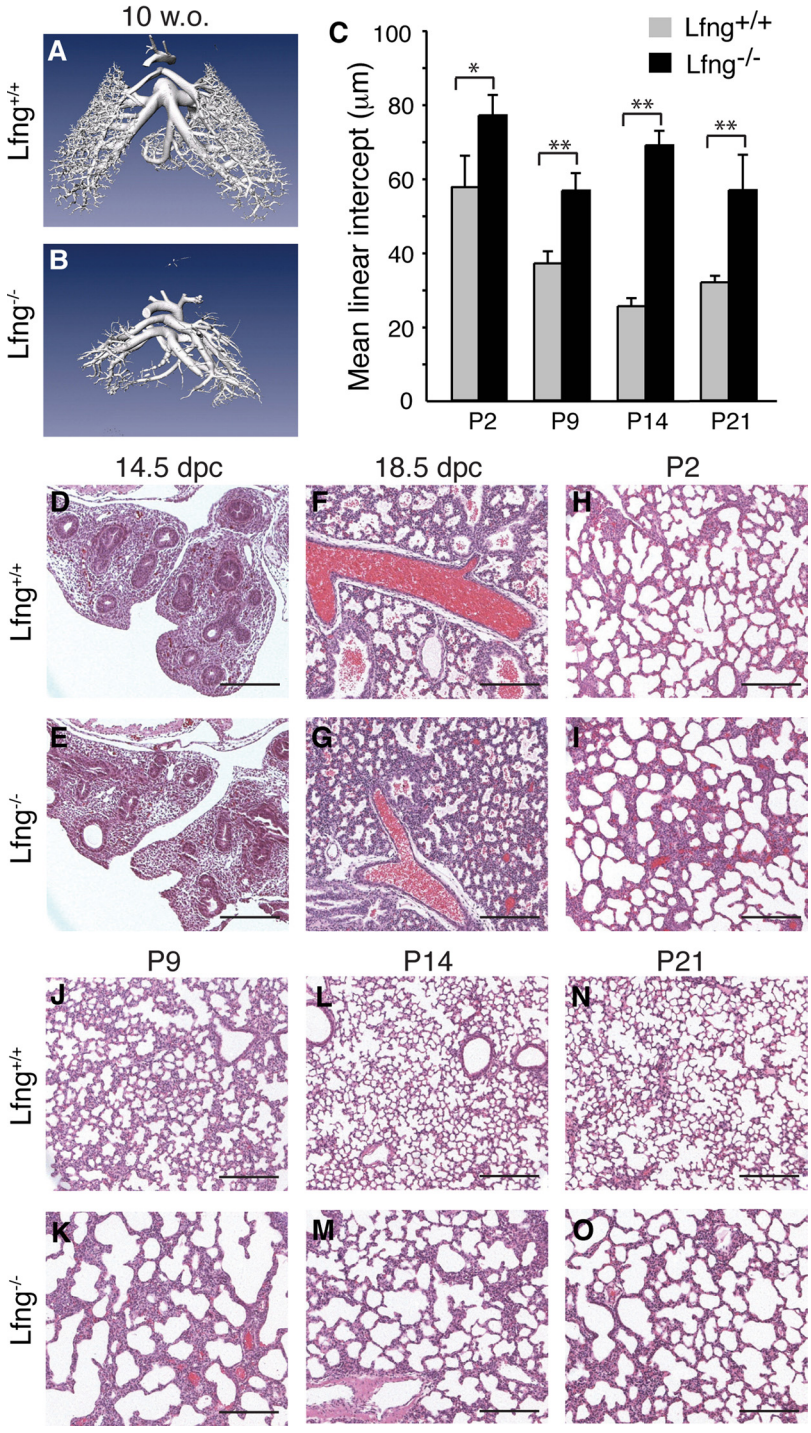

Fig. 2. Abnormal lung development in *Lfng* mutants. *A* and *B*: representative microcomputed tomography images of pulmonary vasculature at 10 wk of age (w.o.). *C*: mean linear intercepts of alveolar septae measured at indicated ages. Values shown are means ± SD. *$P < 0.003$ and **$P < 0.0005$. *D–O*: representative hematoxylin and eosin (H&E)-stained lung sections from *Lfng*$^{+/+}$ (*D*, *F*, *H*, *J*, *L*, and *N*) and *Lfng*$^{-/-}$ (*E*, *G*, *I*, *K*, *M*, and *O*) mice at indicated ages. Note the differences between wild-type and mutant lungs starting at *day 18.5* of gestation (18.5 dpc), at which point *Lfng*$^{-/-}$ lung shows less opened saccules. Postnatal *Lfng*$^{-/-}$ lungs continue to show signs of defective alveolar development, including thickened alveolar walls, lack of alveolar septation, and large alveolar size. Scale bars, 200 μm. P, postnatal day.

analysis using primers 5′-ACCTGTCTGAAGTTGGAGAGTGAG-3′ and 5′-AGCAGTTGGTGAGCACCACATTGC-3′. *Lfng*$^{-/-}$ null status was confirmed at the mRNA level by RT-PCR using primers 5′-GCCTCTCCGAGTACTTCAGTCTAC-3′ and 5′-GGTCATACTCCACAGCCATCTTGC-3′.

Micro-CT imaging. Ten-week-old mice were anesthetized with an intraperitoneal injection of ketamine (50 mg/kg) and xylazine (10 mg/kg). Animals were then intubated orotracheally and connected to a ventilator (TOPO Pressure Controlled Ventilator; Kent Scientific) with tidal volume and respiratory rate adjusted for the weight of the animal as specified by the manufacturer. A median laparotomy was performed, and the diaphragm was removed. Flushing of blood, infusion of contrast agent, fixation of dissected specimens, and imaging by microcomputed tomography (micro-CT) was as previously described (10). Briefly, heparinized PBS (1 unit of heparin/ml) at 37°C was injected into the right ventricle of the heart and drained from the left atrium. The pulmonary circulation was then filled with a radio-opaque silicone rubber (Microfil MV-122; Flow Tech) at a constant pressure of 40 mmHg and left to polymerize for 90 min. Formalin (10%) was instilled in the trachea at a pressure of 20 mmHg, and lungs were excised and maintained in formalin at 4°C for 24 h. Micro-CT data were acquired at 20-μm resolution using a cone beam X-ray scanning system (eXplore Locus SP; General Electric). Seven hundred and twenty views were acquired through a 360° rotation in 2 h with an X-ray tube current of 80 μA and voltage of 80 kVp. The circulation of the lung was visualized as an isointensity surface corresponding to a threshold of ~2,000 Hounsfield units.

Tissue preparation, histology, and mean linear intercept. Lung tissues were collected at designated ages, fixed overnight in 10% buffered neutral formalin or 4% paraformaldehyde, dehydrated, and embedded in paraffin according to standard procedures. Sections (5 μm thick) were cut and stained with hematoxylin and eosin. To measure mean linear intercept (12), slide images were digitally captured, and eight horizontal and six vertical lines were laid over each image. The intercepts of alveolar walls with these lines were counted, and the mean linear intercept was calculated as the sum of the line lengths divided by the sum of the number of intercepts. At least five histological fields from different lobes of each animal and at least two animals of each genotype at each time point were analyzed. All data

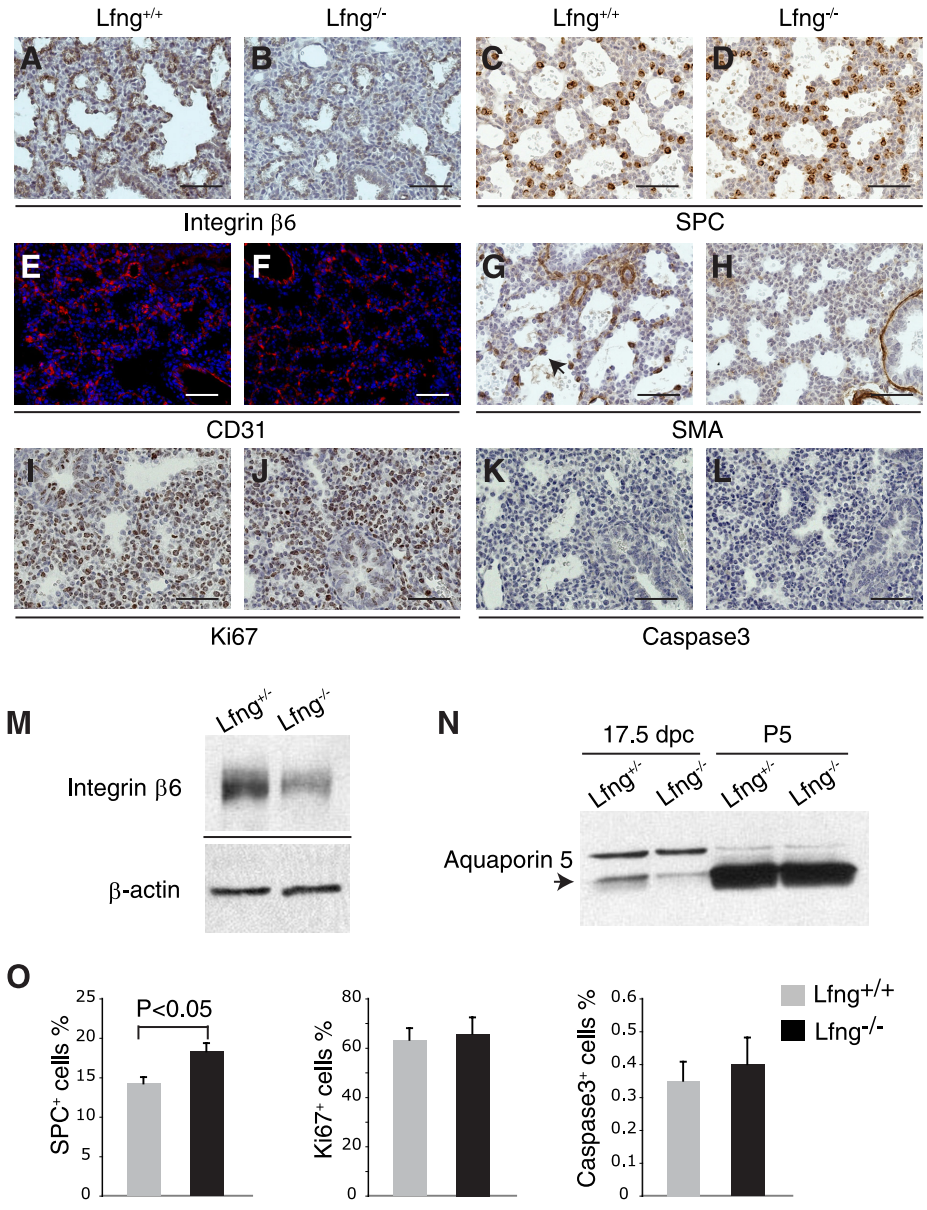

Fig. 3. Immunohistochemical analysis of major cell types in the distal lung at 17.5 dpc. *A–L*: representative photomicrographs of immunostained lung sections at 17.5 dpc with anti-β_6-integrin (*A* and *B*), anti-surfactant protein C (SP-C; *C* and *D*), anti-CD31 (*E* and *F*), anti-smooth muscle actin-α (sma; *G* and *H*), anti-Ki67 (*I* and *J*), and anti-cleaved caspase-3 antibodies (*K* and *L*). Scale bars, 50 μm. *M*: Western blot analysis of β_6-integrin in lung tissues from *Lfng*$^{+/-}$ and *Lfng*$^{-/-}$ mice at 17.5 dpc with β-actin as loading control. *N*: Western blot analysis of aquaporin 5 in lung tissues at 17.5 dpc and P5. Arrow indicates mature form of aquaporin 5. *O*: quantification of immunostaining from 17.5-dpc lung sections. Shown are percentages of SP-C$^+$ cells, Ki67$^+$ cells, and cleaved caspase-3$^+$ cells normalized to the total number of distal lung cells within each image (excluding bronchiolar airways and blood vessels). Data are derived from 2 sections in each of 3 *Lfng*$^{+/-}$ and 3 *Lfng*$^{-/-}$ animals, respectively. Student's *t*-test was performed to assess significance.

are presented as means ± SD. When two groups were compared, Student's *t*-test was used.

β-Gal staining. For β-galactosidase (β-gal) staining, lung tissues were fixed in 2.7% formaldehyde-0.02% Nonidet P-40 in PBS overnight, washed, and infused with 30% sucrose. Tissues were then embedded in optimum cutting temperature compound (OCT), sectioned at 10 μm, and stained with X-gal from 3 h to overnight. All sections were counterstained with eosin.

Immunohistochemistry and Western blot analysis. Lung tissues were prepared as above and stained according to standard protocols. Staining was performed on two sections from each of at least two animals. Presented in the figures are representative photomicrographs. The following antibodies were used: sma (1:200; cat. no. RDI-ACTINabm-A4; Fitzgerald Industries, RDI Division); smooth muscle myosin heavy chain (1:100; cat. no. BT-562; Biomedical Technologies); CD31 (1:50; cat. no. ab28364; Abcam); β_6-integrin (1:20; cat. no. AF2389; R&D Systems); PDGF receptor-α (PDGFRα; 1:200; cat. no. sc-338; Santa Cruz Biotechnology); surfactant protein C (SP-C; 1:200; cat. no. sc-13979; Santa Cruz Biotechnology); T1α/podoplanin (1:100; cat. no. ab11936; Abcam); Ki67 (1:200; cat. no. CRM325; Biocare Medical); cleaved caspase-3 (1:400; cat. no. 9661; Cell Signaling Technology); and Mash1 (1:50; cat. no. 556604; BD Biosciences). For double staining with X-gal and anti-Mash1 antibodies, tissues were whole mount-stained with X-gal and then fixed and embedded in paraffin, sectioned, and subjected to immunostaining. For Western blot analysis, lung tissues were homogenized, lysed in cold lysis buffer [50 mM HEPES, pH 7.4, 150 mM NaCl, 10% glycerol, 1% Triton X-100, 1 mM EGTA, 1.5 mM $MgCl_2$, with complete protease inhibitor (Roche)]. Supernatants were clarified by centrifugation, and total protein was quantified using the Protein Assay Kit (Bio-Rad). Equivalent levels of protein from wild-type and mutant lysates were loaded for Western blots performed according to standard methodology. The primary antibodies used for Western blots were: sma (1:400); β_6-integrin (1:1,000); aquaporin 5 (1:200; cat. no. LS-C40/AN-01; Lifespan Biosciences); elastin (1:100; cat. no. sc-17580; Santa Cruz Biotechnology); and β-actin (1:5,000; cat. no. ab8226; Abcam). Western blot analyses were repeated on multiple lysates with similar results.

RESULTS

Alveolar developmental defect in Lfng mutants. We generated *Lfng* loss-of-function mutants and backcrossed them to FVB mice for six generations. The specific mutation made deletes exon 2, causing a frame shift that destabilizes the resulting mutant mRNA (Fig. 1, *A–E*). In homozygous animals, this mutation results in a fully penetrant rib patterning defect and short-tailed phenotype as seen with other *Lfng* mutant alleles (13, 56). These defects are associated with somitogenesis patterning alterations during embryogenesis (13, 56). As adults, our FVB *Lfng* mutants showed a dramatic defect in lung structure (Fig. 2, *A* and *B*), with altered patterning and reduced vascular branching. To determine how this defect arose, we analyzed late embryonic and postnatal lung development in mutant mice. Before 14.5 dpc, *Lfng* mutant lungs appeared normal. However, a delay in saccule expansion was evident starting at ~16.5 dpc. This was followed by defective alveolar septation. This defect persisted in older animals (Fig. 2, *C–O*). To determine how loss of *Lfng* caused aberrant alveolar development, we tested for expression of cell type-specific markers

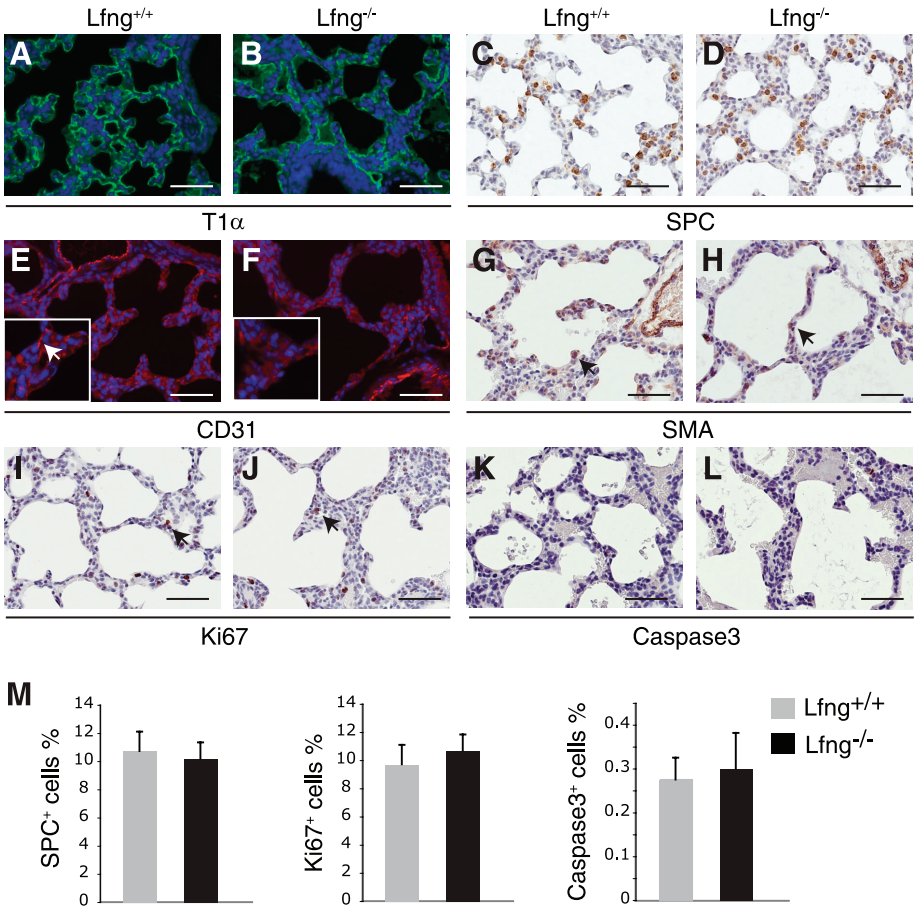

Fig. 4. Immunohistochemical analysis of major cell types in the distal lung during alveolarization. *A–L*: representative photomicrographs of immunostained lung sections at P5 with anti-T1α (*A* and *B*), anti-SP-C (*C* and *D*), anti-CD31 (*E* and *F*), anti-sma (*G* and *H*), anti-Ki67 (*I* and *J*), and anti-cleaved caspase-3 antibodies (*K* and *L*). Scale bars, 50 μm. Arrows point to capillary endothelial cells (*inset* in *E*), sma^+ myofibroblast cells (*G* and *H*), and $Ki67^+$ proliferating cells (*I* and *J*), respectively. *Insets* in *E* and *F* are higher magnification views from the same images. *M*: quantification of immunostaining from P5 lung sections. Shown are percentages of $SP\text{-}C^+$ cells, $Ki67^+$ cells, and cleaved $caspase\text{-}3^+$ cells normalized to the total number of distal lung cells within each image (excluding bronchiolar airways and blood vessels). Data are derived from 2 sections in each of 3 $Lfng^{+/-}$ and 3 $Lfng^{-/-}$ animals, respectively. Student's *t*-test was performed and found no significance ($P > 0.1$).

by immunohistochemistry. Before 16.5 dpc, *Lfng* mutant and wild-type lungs were indistinguishable. In contrast, β_6-integrin, which is induced in wild-type saccular epithelial cells at 17.5 dpc (3), was expressed at lower levels in mutants at this stage (Fig. 3, *A*, *B*, and *M*). SP-C, a marker of type II alveolar epithelial cells, was expressed in a slightly (but significantly) increased number of distal lung cells (Fig. 3, *C*, *D*, and *O*), and the type I alveolar cell marker aquaporin 5 was expressed at lower levels in *Lfng* mutants (data not shown and Fig. 3*N*; Ref. 15). Aquaporin 5 runs on Western blots as a doublet at 17.5 dpc, with a slow migrating precursor form and faster migrating mature form. Interestingly, the level of precursor expression was comparable between wild-type and mutant lungs at 17.5 dpc, whereas the mature form was expressed at much lower levels in mutant lungs (Fig. 3*N*). The Clara cell marker CC10 as well as Mash1 and CGRP, markers of pulmonary neuroendocrine cells (PNEC), were expressed normally in mutant lungs at 17.5 dpc (data not shown). Blood vessel development also appeared normal by anti-CD31 antibodies staining (Fig. 3, *E* and *F*). We next tested for expression of sma, a myofibroblast differentiation marker. At 17.5 dpc, sma is expressed in myofibroblasts of wild-type animals but not in *Lfng* mutant mesenchyme (Fig. 3, *G* and *H*). Finally, the rate of cell proliferation and cell death appeared to be similar in mutant and wild-type lungs at 17.5 dpc (Fig. 3, *I–L* and *O*).

To analyze cell type specification and differentiation in early postnatal life, we performed marker analysis at P5. Expression pattern of T1α, a marker of type I alveolar epithelial cells, was unchanged in the *Lfng* mutant (Fig. 4, *A* and *B*). In addition, mature aquaporin 5 was expressed at approximately similar levels in wild-type and mutant animals at this time point, further indicating that differentiation of alveolar type I cells is only slightly delayed in *Lfng* mutants (Fig. 3*N*). In contrast to 17.5 dpc, where the percentage of SP-C$^+$ cells was higher in *Lfng* mutant lungs, the percentage was similar at P5 (Fig. 4, *C*, *D*, and *M*), indicating normal specification of type II alveolar epithelial cells in the *Lfng* mutant by this stage. Anti-CD31 immunostaining revealed decreased spreading of capillaries along the alveolar wall in *Lfng* mutants (Fig. 4, *E* and *F*), although significant background staining at this time point made it difficult to quantify this effect. As at 17.5 dpc, the number of sma$^+$ myofibroblast cells in mutant lungs was reduced at P5 (Fig. 4, *G* and *H*). Finally, the rate of cell proliferation and cell death were the same in wild-type and mutant lungs at P5 (Fig. 4, *I–L* and *M*).

Myofibroblast differentiation is impaired in Lfng mutant lungs. As the most dramatic defect observed in *Lfng* mutant lungs involved sma induction in the mesenchyme, we analyzed lung myofibroblast differentiation over time. As expected, mesenchymal sma staining was not seen in wild-type or *Lfng* mutant lungs

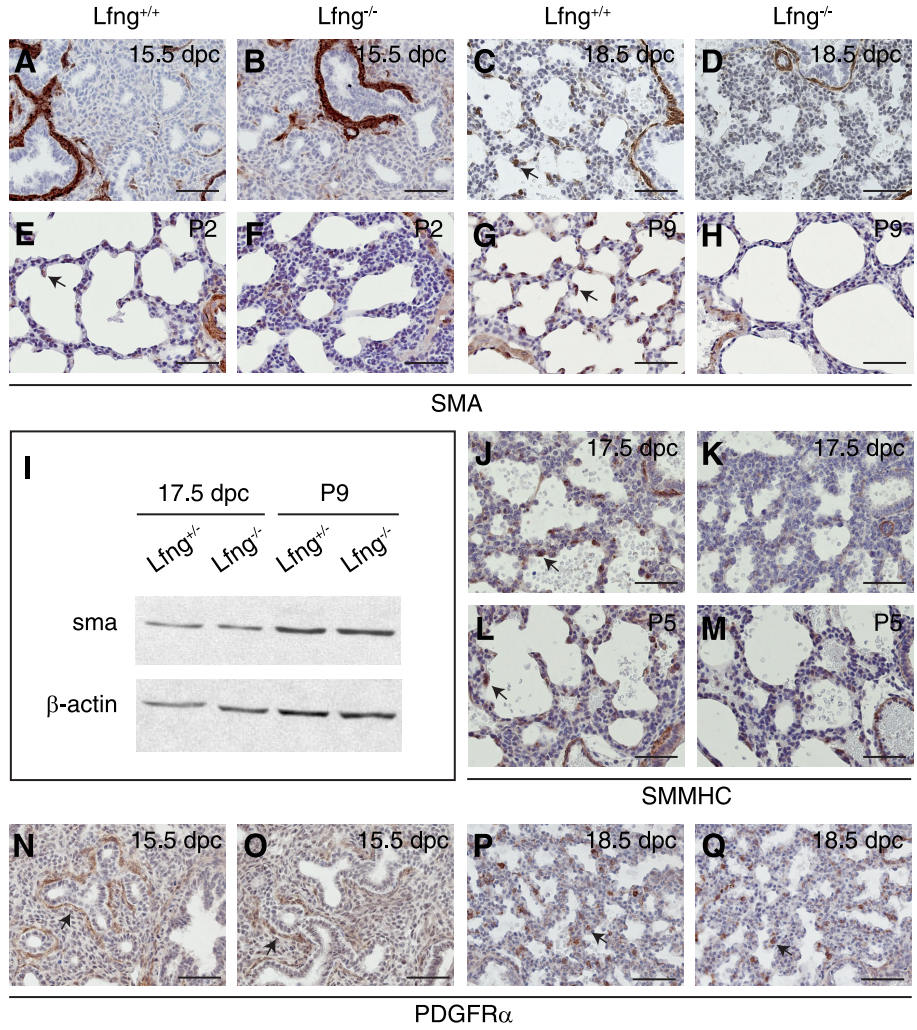

Fig. 5. Defective myofibroblast cell differentiation in *Lfng* mutant lungs. *A–H*: representative immunostaining of lung sections with anti-sma antibody at 15.5 dpc (*A* and *B*), 18.5 dpc (*C* and *D*), P2 (*E* and *F*), and P9 (*G* and *H*). *I*: Western blot analysis of sma in lung tissues from *Lfng*$^{+/-}$ and *Lfng*$^{-/-}$ mice with β-actin as loading control. *J–M*: representative immunostaining of lung sections with anti-smooth muscle myosin heavy chain antibody at 17.5 dpc (*J* and *K*) and P5 (*L* and *M*). *N–Q*: representative immunostaining of lung sections with anti-PDGF receptor-α (PDGFRα) antibody at 15.5 dpc (*N* and *O*) and 18.5 dpc (*P* and *Q*). Arrows in *C*, *E*, *G*, *J*, and *L* indicate myofibroblast cells located at the growing septae. Arrows in *N* and *O* point at clusters of PDGFRα-positive cells surrounding the distal bronchiolar airways. Arrows in *P* and *Q* point at PDGFRα-positive cells migrated to alveolar walls. Scale bars, 50 μm.

at 15.5 dpc (Fig. 5, *A* and *B*). As noted above, sma expression was observed in wild-type but not mutant mesenchyme at 17.5 dpc (Fig. 3, *G* and *H*) and at P5 (Fig. 4, *G* and *H*). Sma staining was still evident in smooth muscle cells surrounding the large airways and blood vessels in mutant lungs at each of these time points. At P2 and P9, sma staining was found in myofibroblast cells that had migrated to branch or septation points in the developing alveoli of wild-type lungs (Fig. 5, *E* and *G*). In contrast, sma was expressed at a low level in a small number of *Lfng* mutant mesenchymal cells at both time points. Most of these were trapped within multilayered walls separating large alveoli (Fig. 5, *F* and *H*). By Western blot analysis, overall expression of sma was not significantly changed (Fig. 5*I*). This was likely due to high-level sma expression in smooth muscle cells surrounding the large airways and blood vessels of wild-type and mutant mice.

We next stained for myofibroblast differentiation using antibodies against smooth muscle myosin heavy chain. As with sma, this protein is expressed in smooth muscle cells surrounding the large airways and blood vessels in wild-type and mutant lungs and in myofibroblasts at the branch points in the distal lungs of wild-type animals at 17.5 dpc and P5 (Fig. 5, *J* and *L*). In contrast, only low-level smooth muscle myosin heavy chain expression was observed in a small number of *Lfng* mutant mesenchymal cells at these time points (Fig. 5, *K* and *M*). Myofibroblast progenitor cells in the developing distal lung require PDGFRα (31). This receptor was expressed similarly in wild-type and mutant lungs during late embryogenesis, indicating that differentiation but not specification or spreading of myofibroblast progenitors is affected in *Lfng*$^{-/-}$ lungs (Fig. 5, *N–Q*).

Myofibroblasts express and deposit elastin, which is critical for alveogenesis and lung function (4). We therefore analyzed elastin expression and deposition in wild-type and mutant animals using Verhoeff stain. At P5, a small number of elastic fibers were noted in both wild-type and mutant lungs (Fig. 6, *A* and *B*). By P14 and at 6 wk of age, elastin is strongly expressed and highly localized to alveolar walls in wild-type animals (Fig. 6, *C* and *E*). In contrast, elastin deposition is altered in *Lfng* mutants. At P14, few elastic fibers were evident in mutant lungs (Fig. 6*D*), and by 6 wk of age, accumulation was noted in mesenchymal cells trapped within multilayered walls (Fig. 6*F*). Altered elastin deposition was associated with slightly lower expression in mutants at P9 but elevated expression at P42 (Fig. 6*G*). Next, we used Masson trichrome stain to detect collagen fibers. In 6-wk-old wild-type lungs, thin collagen fibers were localized to within alveolar walls as expected (Fig. 6*H*). In contrast, *Lfng* mutant lungs at 6 wk contained large collagenous deposits/fibers in most alveolar walls (Fig. 6*I*). These alterations were not associated with increased apoptosis in mutant lungs (data not shown).

Lfng is expressed in PNEC and alveolar progenitor cells. *Lfng* and other Notch pathway components are expressed in the developing mouse lung (42, 54). To determine precisely when and where *Lfng* was expressed, we used *Lfng*^{lacZ} reporter mice (56). At 16.5 and 18.5 dpc, Lfng was expressed in the distal lung, including saccular cells (54) and cells within the mesenchyme (Fig. 7, *A–C*). Cells expressing the highest level were found within the NEB. These and isolated cells with strong X-gal staining were identified as PNEC, as they stained positive for X-gal and Mash1 (Fig. 7*D*). Expression within the

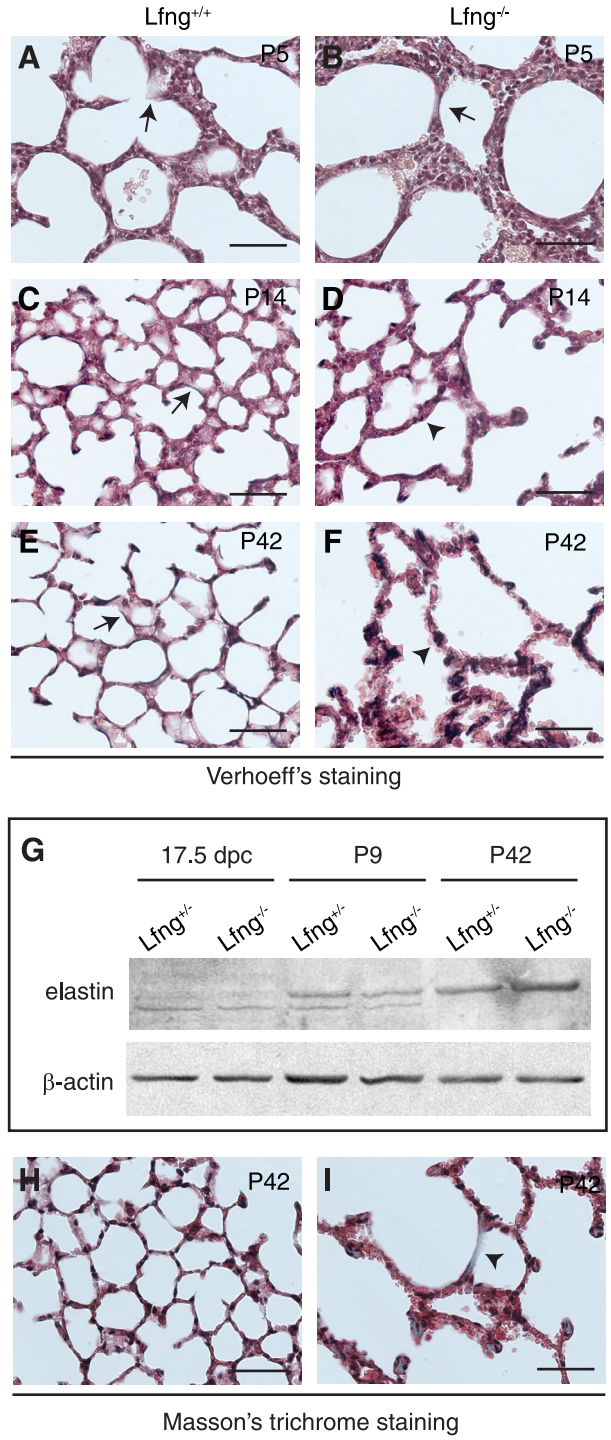

Fig. 6. Altered elastogenesis and collagen deposition in *Lfng* mutant lungs. *A–F*: representative photomicrographs showing Verhoeff staining of lung sections at P5 (*A* and *B*), P14 (*C* and *D*), and P42 (*E* and *F*). Arrows in *C* and *E* point at continuous elastic fibers (stained in dark brown) in wild-type lungs. Arrowheads in *D* and *F* indicate accumulation of disorganized elastic fibers in *Lfng*$^{-/-}$ mutant lungs. *G*: Western blot analysis of elastin in lung tissues from *Lfng*$^{+/-}$ and *Lfng*$^{-/-}$ mice. *H* and *I*: representative photomicrographs of Masson trichrome staining in P42 lung sections showing increased deposition of collagen in *Lfng*$^{-/-}$ mutant (stained in green, arrowhead in *I*). This increased deposition was observed in most areas of mutant lungs. Scale bars, 50 μm.

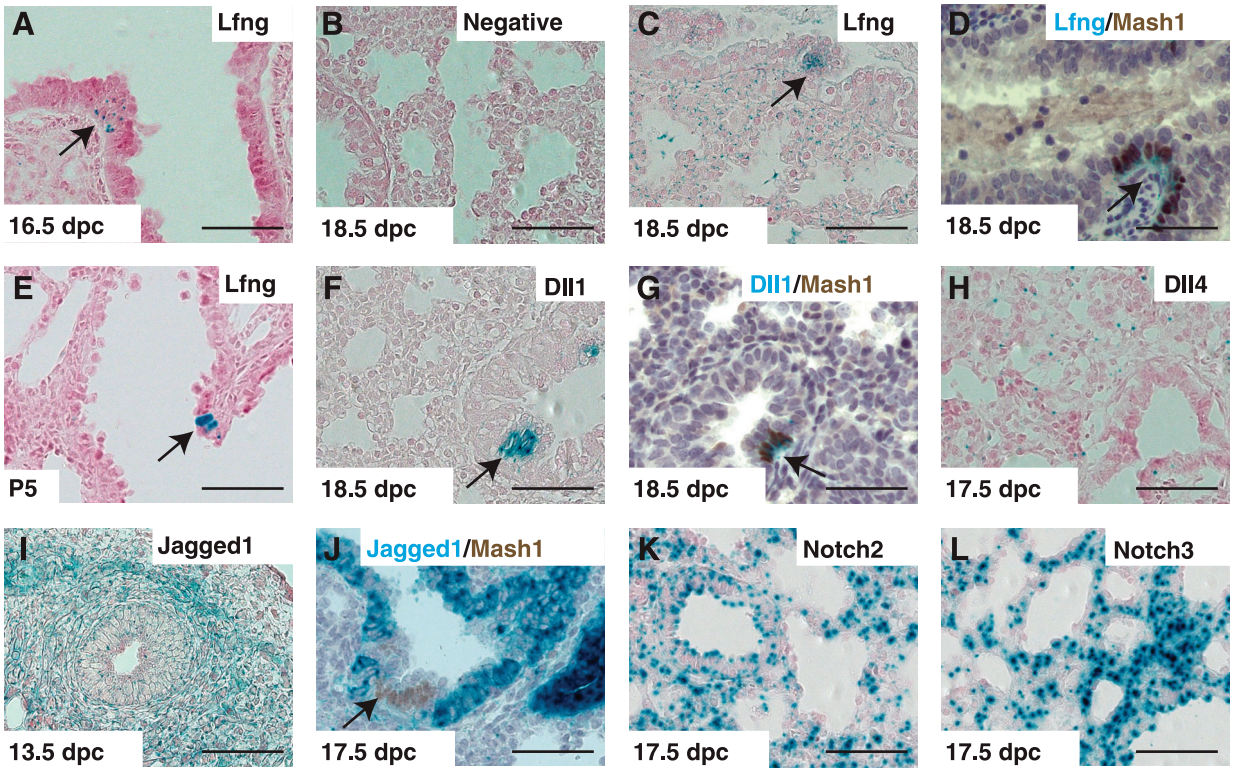

Fig. 7. Expression of *Lfng*, Notch ligands, and receptors in developing lungs. Shown are representative photomicrographs of X-galactosidase (X-gal) staining in lung sections from $Lfng^{lacZ/lacZ}$ (*A* and *C–E*), wild-type (*B*), $Dll1^{lacZ/+}$ (*F* and *G*), $Dll4^{lacZ/+}$ (*H*), $Jagged1^{\beta\text{-}geo/+}$ (*I* and *J*), $Notch2^{\beta\text{-}geo/+}$ (*K*), and $Notch3^{\beta\text{-}geo/+}$ (*L*) mice at indicated developmental stages. Double staining of X-gal (stained in blue) and anti-Mash1 (stained in brown) are shown in *D*, *G*, and *J*. Arrows point to neuroepithelial bodies (NEBs). Scale bars, 50 μm. Dll1/4, Delta-like ligands.

NEB was observable in $Lfng^{lacZ/+}$ mice (data not shown), whereas staining in other cells of the distal lung was consistently observed only in $Lfng^{lacZ/lacZ}$ homozygotes. At P5, $Lfng^{lacZ}$ was still expressed in NEBs but was also seen in endothelial cells of large pulmonary veins (Fig. 7*E* and data not shown).

We next tested for Notch ligand and receptor expression. In $Dll1^{lacZ/+}$ mice (22), LacZ is expressed in PNEC throughout lung development (Ref. 42; Fig. 7, *F* and *G*) and also in vascular endothelial cells after P5 (Ref. 42 and data not shown). Expression of *Lfng* and *Dll1* in PNEC is not surprising, since both genes are induced by Mash1 (16, 40). In $Dll4^{lacZ/+}$ mice at 17.5 dpc, X-gal-positive cells were found in endothelial cells scattered throughout the mesenchyme and in PNEC (Fig. 7*H*; Ref. 11). Next, to define Jagged1 expression, we made $Jagged1^{\beta\text{-}geo/+}$ reporter mice using a publically available ES cell line obtained in a screen to target genes encoding membrane-anchored or -secreted proteins (33). The specific ES line used has a transmembrane-anchored β-geo gene fused in-frame with sequences coding for the first 13 EGF repeats of Jagged1 (Fig. 8*A*). In this mouse, LacZ staining was noted in pulmonary veins and arteries throughout development, in mesenchymal cells during early embryonic lung development, and in bronchiolar epithelial cells starting at ~16.5 dpc (Fig. 7, *I* and *J*). Bronchiolar epithelial expression was notably interrupted at the NEB, where PNEC and variant Clara cells were clearly $LacZ^-$ (see arrow in Fig. 7*J*). By in situ hybridization and immunohistochemistry, strong Notch1 expression was noted at 14.5 and 16.5 dpc in distal endoderm and in bronchiolar cells, respectively (data not shown and Ref. 23). Finally, we used ES cells from the same gene trap screen to generate Notch2 and Notch3 reporter mice, $Notch2^{\beta\text{-}geo/+}$ and $Notch3^{\beta\text{-}geo/+}$, respectively (Ref. 33; Fig. 8, *B* and *C*). X-gal staining for both genes was observed in lung mesenchyme and airway epithelium at 17.5 dpc, and this expression persisted to P5 and beyond (Fig. 7, *K* and *L*, and data not shown). As expression of both receptors was strong, and in many cell types, it was difficult to exclude expression in any specific lineage of the distal lung.

Altered myofibroblast differentiation is associated with loss of Notch signaling. As noted above, Notch2 and Notch3 are expressed in multiple cell types of the distal lung during saccule and alveolar development, and these genes are known to control myofibroblast differentiation in vitro (25, 39). We next analyzed lungs of $Notch2^{\beta\text{-}geo/+}$, $Notch3^{\beta\text{-}geo/\beta\text{-}geo}$, as well as $Notch2^{\beta\text{-}geo/+}Notch3^{\beta\text{-}geo/\beta\text{-}geo}$ double-mutant mice at 17.5 dpc to test for myofibroblast differentiation using sma as a marker. As in wild-type mice, myofibroblast cells were clearly present in the mesenchyme of $Notch2^{\beta\text{-}geo/+}$ and $Notch3^{\beta\text{-}geo/\beta\text{-}geo}$ mutant lungs at this time point. In contrast, mesenchymal sma staining was either absent or reduced in $Notch2^{\beta\text{-}geo/+}Notch3^{\beta\text{-}geo/\beta\text{-}geo}$ double-mutant lungs at 17.5 dpc (Fig. 9, *A–C*). In contrast to the situation in *Lfng* mutant mice, we did not detect any delay in distal lung epithelial differentiation in $Notch2^{\beta\text{-}geo/+}Notch3^{\beta\text{-}geo/\beta\text{-}geo}$ double-mutant mice (data not shown). Whereas most of the $Notch2^{\beta\text{-}geo/+}Notch3^{\beta\text{-}geo/\beta\text{-}geo}$ mutants died shortly after birth, altered alveolar development was observed in three of the six compound mutant mice that survived weaning (Fig. 9, *D–F*).

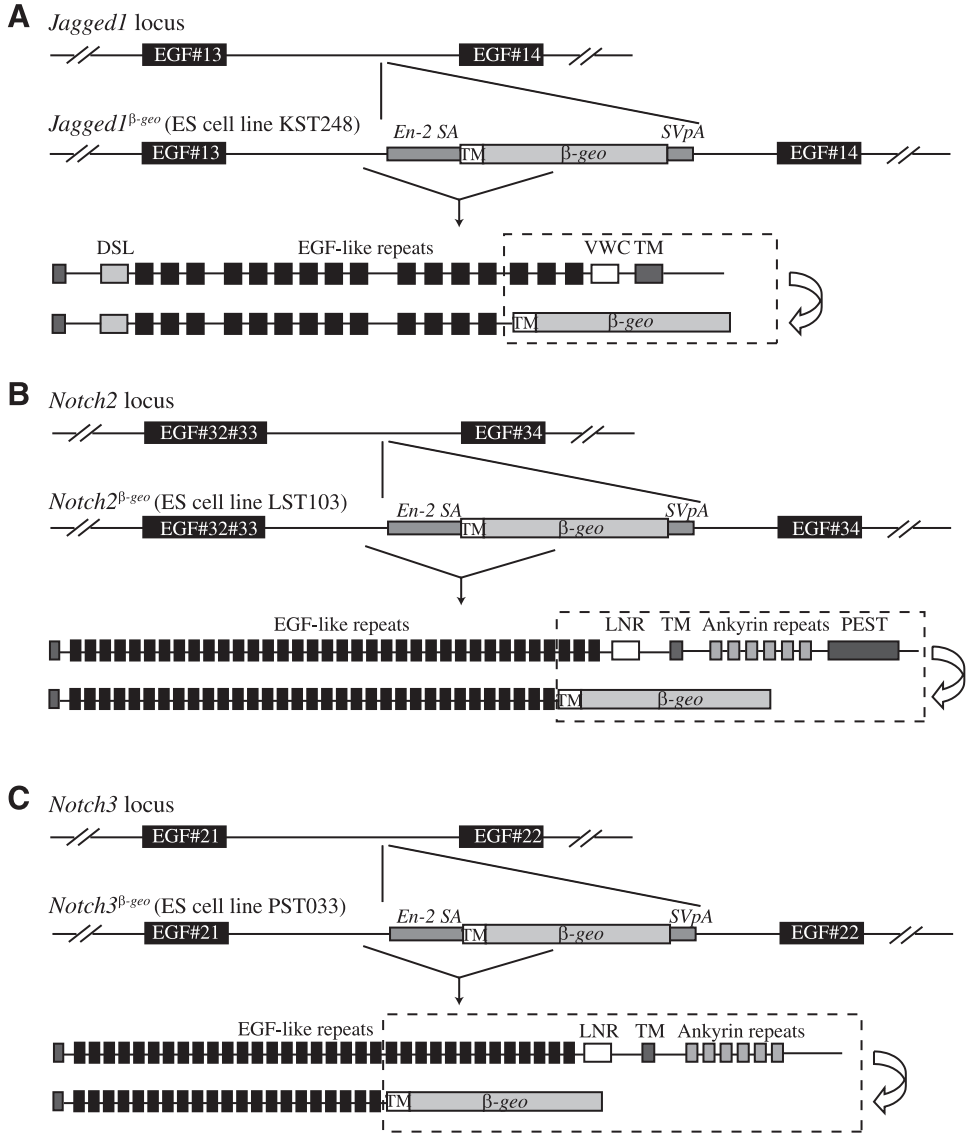

Fig. 8. Genomic structure of *Jagged1*, *Notch2*, and *Notch3* mutant alleles. *A*: *Jagged1* was targeted in a secretory gene trap screen using a vector containing β-geo preceded by a transmembrane domain and flanked by a splicing acceptor and polyadenylation sites. The construct integrated into an intron between exons coding for EGF repeats #13 and #14, respectively, resulting in a truncated Jagged1 fused to β-geo. *B* and *C*: using the same vector, *Notch2* and *Notch3* were targeted to produce β-geo fusion proteins with 33 and 21 EGF repeats, respectively, of their extracellular domains. Gene trap ES cell lines KST248 (Jagged1), LST103 (Notch2), and PST033 (Notch3) were obtained from BayGenomics. *En-2 SA*, Engrailed-2 splice acceptor sequence; *SVpA*, polyA addition sequence from simian virus (SV40); *DSL*, Delta/Serrate/Lag-2 domain; VWCTM, Von Willebrand factor C domain, transmembrane domain; *LNR*, Lin-12 Notch repeat-containing region; PEST, Proline/Glutamic acid/Serine/Threonine rich sequences.

These data suggest that Notch2 and Notch3 may function redundantly to control myofibroblast differentiation in the developing lung mesenchyme. Indeed, as noted above, various Notch receptors have been shown to regulate myofibroblast differentiation in vitro or during induction of lung fibrosis in vivo, although the specific receptor involved, as well as whether Notch signaling promoted or suppressed sma expression, was dependent on the starting cell type and the inducer (25, 32, 39). Therefore, to directly test whether canonical Notch signaling is required for myofibroblast differentiation in the developing lung, we used *RBPJκ*$^{flox/flox}$ mutant mice with the DOX-inducible *ROSA26*-rtTA$^{/+}$;tetO-*CRE*$^{/+}$ deletion system to inactivate *RBPJκ* starting at 14.5 dpc. Deletion at this time completely blocked the appearance of sma^{+} myofibroblasts by 18.5 dpc (Fig. 9, *G* and *H*) while having no apparent effect on the development of SP-C^{+} alveolar epithelial cells (Fig. 9, *I* and *J*) or smooth muscle cells surrounding the major airways and blood vessels (Fig. 9, *G* and *H*). Although DOX-treated RBPJκ conditional mutants typically died shortly after birth, reduced sma staining was also observed in mutant pups at P0 with morphologically normal lungs (Fig. 9, *K* and *L*). In contrast, SP-C and T1α staining was unchanged in these pups (Fig. 9, *M–P*).

DISCUSSION

The lung is a highly specialized organ that facilitates rapid and efficient oxygenation of blood. This is achieved at the interface of alveoli and microcapillaries, each organized in a complex labyrinth of interconnected thin-walled sacs and tubes (4). During fetal and postnatal development, these structures are formed through septation and growth of saccules as well as through simultaneous branching and growth of blood vessels. These events must occur in a highly coordinated manner and under conditions where the lung is subjected to elastic forces associated with breathing. Notch signaling regulates lung epithelial cell fate (6, 19, 23, 28, 46, 52, 53) and blood vessel patterning (2, 17). In addition, Notch signaling has been shown to regulate myofibroblast differentiation in vitro (25, 32, 39) and myofibroblast induction during fibrosis in vivo (32). Here,

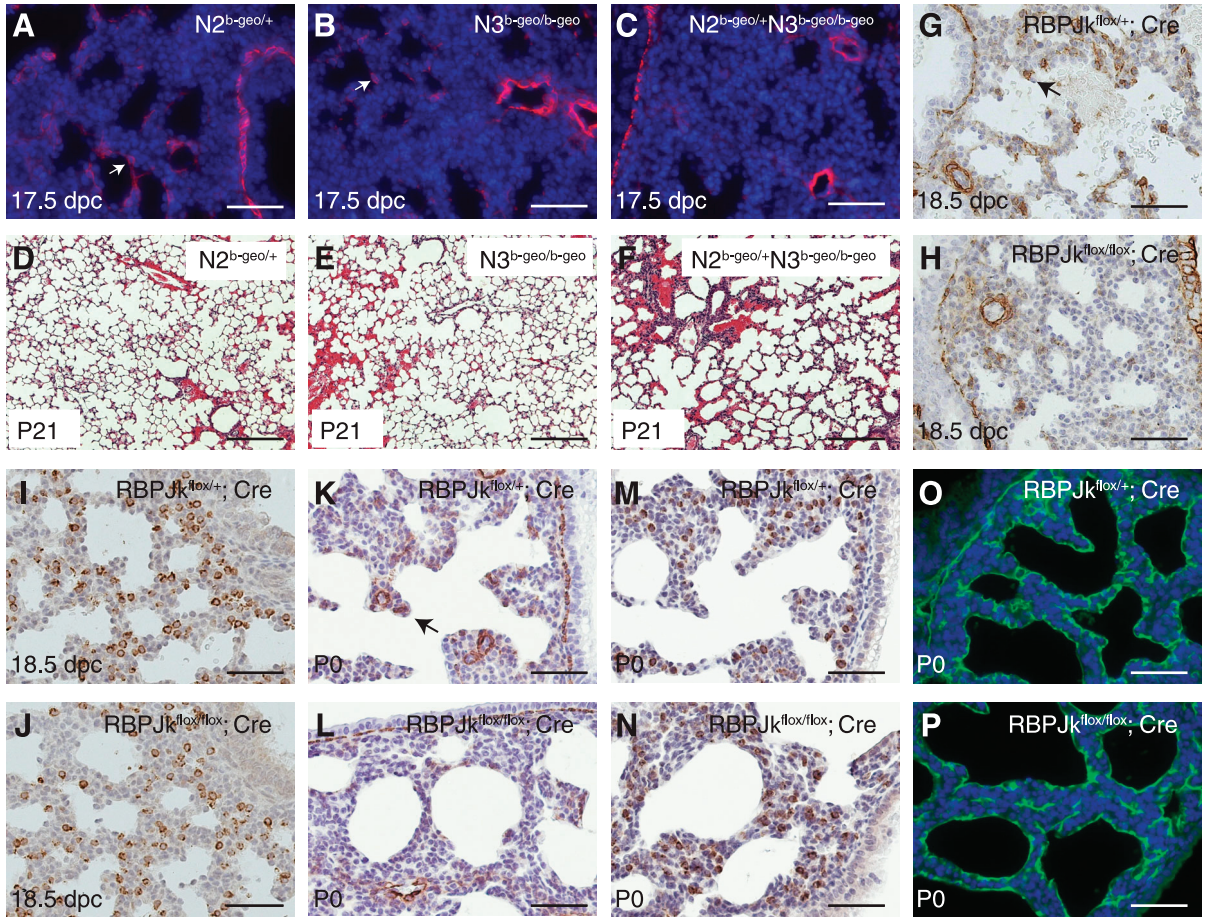

Fig. 9. Defective myofibroblast cell differentiation in *Notch2/3* (N2/N3) compound mutants and *RBPJκ* inducible knockout mice. *A–C*: representative photomicrographs of anti-sma immunofluorescence staining in lung sections from $Notch2^{\beta\text{-}geo/+}$, $Notch3^{\beta\text{-}geo/\beta\text{-}geo}$, and $Notch2^{\beta\text{-}geo/+}Notch3^{\beta\text{-}geo/\beta\text{-}geo}$ embryos at 17.5 dpc. *D–F*: representative photomicrographs of H&E staining of lung sections from $Notch2^{\beta\text{-}geo/+}$, $Notch3^{\beta\text{-}geo/\beta\text{-}geo}$, and $Notch2^{\beta\text{-}geo/+}Notch3^{\beta\text{-}geo/\beta\text{-}geo}$ mice at P21. *G–J*: representative photomicrographs of anti-sma staining (*G* and *H*) and anti-SP-C staining (*I* and *J*) in lung sections from doxycycline-exposed *ROSA26-rtTA*; *tetO-Cre*; $RBPJ\kappa^{flox/+}$ and *ROSA-rtTA*; *tetO-Cre*; $RBPJ\kappa^{flox/flox}$ embryos at 18.5 dpc. Pregnant females containing these embryos were given doxycycline-containing drinking water from 14.5 to 18.5 dpc. *K–P*: representative photomicrographs of anti-sma staining (*K* and *L*), anti-SP-C staining (*M* and *N*), and anti-T1α staining (*O* and *P*) in lung sections from doxycycline-exposed *ROSA26-rtTA*; *tetO-Cre*; $RBPJ\kappa^{flox/+}$ and *ROSA-rtTA*; *tetO-Cre*; $RBPJ\kappa^{flox/flox}$ pups at P0. Arrows in *A*, *B*, *G*, and *K* indicate sma^+ myofibroblast cells. Scale bars represent 50 μm in *A–C* and *G–P* and 200 μm in *D–F*.

we report that alveolar development is impaired in *Lfng* mutant mice, starting in the saccule phase of fetal lung development, with impaired differentiation of myofibroblasts, accompanied by a modest delay of type I alveolar epithelial cell differentiation. Lfng, like all Fringe proteins, enhances Notch receptor activation by Delta/Dll ligands and suppresses activation by Serrate/Jagged ligands (20). In this context, therefore, Lfng could either be enhancing or suppressing Notch activation.

We have approached this question in two ways. First, Notch2 and Notch3 are both highly expressed during saccular development in the distal lung. We have therefore generated and studied $Notch2^{\beta\text{-}geo/+}$ and $Notch3^{\beta\text{-}geo/\beta\text{-}geo}$ mutants as well as $Notch2^{\beta\text{-}geo/+}Notch3^{\beta\text{-}geo/\beta\text{-}geo}$ compound mutants. Myofibroblast differentiation was impaired in $Notch2^{\beta\text{-}geo/+}Notch3^{\beta\text{-}geo/\beta\text{-}geo}$ compound mutant embryos but not in single mutants, suggesting that these receptors function redundantly to induce myofibroblast differentiation. Second, we tested whether conditional deletion of *RBPJκ* caused a similar impairment of myofibroblast differentiation. Indeed, disruption of all canonical Notch signaling in this way prevented distal lung myofibroblast differentiation under conditions where epithelial SP-C induction in saccule cells and smooth muscle development around large airways and blood vessels were not affected. $Notch^{IC}$-RBPJκ complex can directly bind to and activate the *sma* gene promoter (38). The simplest model to explain our data would therefore be that Lfng functions within myofibroblast progenitor cells to enhance activation of Notch2 and Notch3 by Dll-family ligands. In this case, Dll4 expressed in endothelial cells of the distal lung would be the strongest candidate ligand. To address this model directly, lineage-specific deletion of *Lfng*, *Notch2*, *Notch3*, as well as *Dll4* (if feasible) will be required.

Although myofibroblast cell differentiation was impaired in *Lfng* mutant mice, this was not the only lung phenotype observed. We also found a small but reproducible delay in saccule epithelial cell development that appeared to correct itself by birth. This delay may be related to low-level expression of *Lfng* in saccular cells, which could enhance or suppress Notch signaling in developing alveolar type II or type I cells late in embryogenesis and early in postnatal life. Alternatively, *Lfng* may not function within saccular or alveolar epithelial progenitor cells, and delayed differentiation of these cells may

be secondary to impaired differentiation of myofibroblasts or other mesenchymal cell types (8). Indeed, previous studies suggest that Notch signaling is not required for specification of alveolar epithelial cells (53). *Lfng* could also function in saccular cells to prevent Notch activation by Jagged ligands. In this case, ectopic Notch activation may well occur in *Lfng* mutant saccular cells, and such signaling is known to block alveolar epithelial differentiation (7, 19). Finally, we have described a Notch expression boundary at the NEB, where Dll1 and Dll4 are expressed in PNEC cells, Jagged1 is expressed in neighboring epithelial cells, and Notch receptors are expressed in multiple cell types. The NEB and related bronchoalveolar junctions are thought to represent stem cell niches (26) as well as signaling centers that control distal lung development (36). Although *Lfng* mutation does not affect specification of PNEC as judged by expression of Mash1 and CGRP, by analogy to its role in central nervous system development, it may affect stem cell differentiation kinetics in this context (37). Conditional mutant analysis will be required to probe for such functions. In summary, we have shown that Lfng-mediated Notch signaling is required for timely differentiation of myofibroblast cells in the lung and that a delay in this event caused by loss of *Lfng* or Notch2/3 signaling results in defective alveolar septation and elastogenesis.

ACKNOWLEDGMENTS

We thank Martin Post, Fred Keeley, Jeff Wigle, colleagues in the histology lab at the Hospital for Sick Children, and members of the Egan lab. We also thank BayGenomics for the mutant ES cell lines used in this study as well as Scott Pownall and Tak Mak for the knockout vector used to generate *Lfng* mutant mice and advice on gene targeting. We thank Nichola Wigle, Linda Wei, Julie Panakos, and Susan Quaggin (Samuel Lunenfeld Research Institute) for their assistance with generation of, or access to, mutant mice. We thank T. Honjo (Kyoto University, Kyoto, Japan) for providing us with *RBPJκ*$^{flox/flox}$ mice. We gratefully acknowledge V. Eremina and M. Gertenstein (Samuel Lunenfeld Research Institute) and H. Su (Hospital for Sick Children) for their technical assistance.

GRANTS

K. Xu was supported by a Canadian Institutes of Health Research fellowship. S. E. Egan's lab has been supported by funds from the Canadian Cancer Society Research Institute and from the United States Army Department of Defense. T. Gridley was supported by National Institute of Neurological Disorders and Stroke Grant NS-036437.

DISCLOSURES

No conflicts of interest are declared by the author(s).

REFERENCES

1. **Belteki G, Haigh J, Kabacs N, Haigh K, Sison K, Costantini F, Whitsett J, Quaggin SE, Nagy A.** Conditional and inducible transgene expression in mice through the combinatorial use of Cre-mediated recombination and tetracycline induction. *Nucleic Acids Res* 33: e51, 2005.
2. **Benedito R, Roca C, Sorensen I, Adams S, Gossler A, Fruttiger M, Adams RH.** The notch ligands Dll4 and Jagged1 have opposing effects on angiogenesis. *Cell* 137: 1124–1135, 2009.
3. **Breuss JM, Gallo J, DeLisser HM, Klimanskaya IV, Folkesson HG, Pittet JF, Nishimura SL, Aldape K, Landers DV, Carpenter W, Gillett N, Sheppard D, Matthay MA, Albelda SM, Kramer RH, Pytela R.** Expression of the beta 6 integrin subunit in development, neoplasia and tissue repair suggests a role in epithelial remodeling. *J Cell Sci* 108: 2241–2251, 1995.
4. **Burri PH.** Structural aspects of postnatal lung development - alveolar formation and growth. *Biol Neonate* 89: 313–322, 2006.
5. **Cohen B, Bashirullah A, Dagnino L, Campbell C, Fisher WW, Leow CC, Whiting E, Ryan D, Zinyk D, Boulianne G, Hui CC, Gallie B, Phillips RA, Lipshitz HD, Egan SE.** Fringe boundaries coincide with Notch-dependent patterning centres in mammals and alter Notch-dependent development in *Drosophila*. *Nat Genet* 16: 283–288, 1997.
6. **Collins BJ, Kleeberger W, Ball DW.** Notch in lung development and lung cancer. *Semin Cancer Biol* 14: 357–364, 2004.
7. **Dang TP, Eichenberger S, Gonzalez A, Olson S, Carbone DP.** Constitutive activation of Notch3 inhibits terminal epithelial differentiation in lungs of transgenic mice. *Oncogene* 22: 1988–1997, 2003.
8. **Deimling J, Thompson K, Tseu I, Wang J, Keijzer R, Tanswell AK, Post M.** Mesenchymal maintenance of distal epithelial cell phenotype during late fetal lung development. *Am J Physiol Lung Cell Mol Physiol* 292: L725–L741, 2007.
9. **Doi H, Iso T, Sato H, Yamazaki M, Matsui H, Tanaka T, Manabe I, Arai M, Nagai R, Kurabayashi M.** Jagged1-selective notch signaling induces smooth muscle differentiation via a RBP-Jkappa-dependent pathway. *J Biol Chem* 281: 28555–28564, 2006.
10. **Dorr A, Sled JG, Kabani N.** Three-dimensional cerebral vasculature of the CBA mouse brain: a magnetic resonance imaging and micro computed tomography study. *Neuroimage* 35: 1409–1423, 2007.
11. **Duarte A, Hirashima M, Benedito R, Trindade A, Diniz P, Bekman E, Costa L, Henrique D, Rossant J.** Dosage-sensitive requirement for mouse Dll4 in artery development. *Genes Dev* 18: 2474–2478, 2004.
12. **Dunnill MS.** Evaluation of a simple method of sampling the lung for quantitative histological analysis. *Thorax* 19: 443–448, 1964.
13. **Evrard YA, Lun Y, Aulehla A, Gan L, Johnson RL.** Lunatic fringe is an essential mediator of somite segmentation and patterning. *Nature* 394: 377–381, 1998.
14. **Fortini ME.** Notch signaling: the core pathway and its posttranslational regulation. *Dev Cell* 16: 633–647, 2009.
15. **Funaki H, Yamamoto T, Koyama Y, Kondo D, Yaoita E, Kawasaki K, Kobayashi H, Sawaguchi S, Abe H, Kihara I.** Localization and expression of AQP5 in cornea, serous salivary glands, and pulmonary epithelial cells. *Am J Physiol Cell Physiol* 275: C1151–C1157, 1998.
16. **Gohlke JM, Armant O, Parham FM, Smith MV, Zimmer C, Castro DS, Nguyen L, Parker JS, Gradwohl G, Portier CJ, Guillemot F.** Characterization of the proneural gene regulatory network during mouse telencephalon development. *BMC Biol* 6: 15, 2008.
17. **Gridley T.** Notch signaling in vascular development and physiology. *Development* 134: 2709–2718, 2007.
18. **Gridley T.** The long and short of it: somite formation in mice. *Dev Dyn* 235: 2330–2336, 2006.
19. **Guseh JS, Bores SA, Stanger BZ, Zhou Q, Anderson WJ, Melton DA, Rajagopal J.** Notch signaling promotes airway mucous metaplasia and inhibits alveolar development. *Development* 136: 1751–1759, 2009.
20. **Haines N, Irvine KD.** Glycosylation regulates Notch signalling. *Nat Rev Mol Cell Biol* 4: 786–797, 2003.
21. **Han H, Tanigaki K, Yamamoto N, Kuroda K, Yoshimoto M, Nakahata T, Ikuta K, Honjo T.** Inducible gene knockout of transcription factor recombination signal binding protein-J reveals its essential role in T versus B lineage decision. *Int Immunol* 14: 637–645, 2002.
22. **Hrabe de Angelis M, McIntyre J 2nd, Gossler A.** Maintenance of somite borders in mice requires the Delta homologue DII1. *Nature* 386: 717–721, 1997.
23. **Ito T, Udaka N, Yazawa T, Okudela K, Hayashi H, Sudo T, Guillemot F, Kageyama R, Kitamura H.** Basic helix-loop-helix transcription factors regulate the neuroendocrine differentiation of fetal mouse pulmonary epithelium. *Development* 127: 3913–3921, 2000.
24. **Johnston SH, Rauskolb C, Wilson R, Prabhakaran B, Irvine KD, Vogt TF.** A family of mammalian Fringe genes implicated in boundary determination and the Notch pathway. *Development* 124: 2245–2254, 1997.
25. **Kennard S, Liu H, Lilly B.** Transforming growth factor-beta (TGF-β1) down-regulates Notch3 in fibroblasts to promote smooth muscle gene expression. *J Biol Chem* 283: 1324–1333, 2008.
26. **Kim CF, Jackson EL, Woolfenden AE, Lawrence S, Babar I, Vogel S, Crowley D, Bronson RT, Jacks T.** Identification of bronchioalveolar stem cells in normal lung and lung cancer. *Cell* 121: 823–835, 2005.
27. **Kim N, Vu TH.** Parabronchial smooth muscle cells and alveolar myofibroblasts in lung development. *Birth Defects Res C Embryo Today* 78: 80–89, 2006.
28. **Kong Y, Glickman J, Subramaniam M, Shahsafaei A, Allamneni KP, Aster JC, Sklar J, Sunday ME.** Functional diversity of *notch* family genes in fetal lung development. *Am J Physiol Lung Cell Mol Physiol* 286: L1075–L1083, 2004.
29. **Kopan R, Ilagan MX.** The canonical Notch signaling pathway: unfolding the activation mechanism. *Cell* 137: 216–233, 2009.

30. **Lakso M, Pichel JG, Gorman JR, Sauer B, Okamoto Y, Lee E, Alt FW, Westphal H.** Efficient in vivo manipulation of mouse genomic sequences at the zygote stage. *Proc Natl Acad Sci USA* 93: 5860–5865, 1996.
31. **Lindahl P, Bostrom H, Karlsson L, Hellstrom M, Kalen M, Betsholtz C.** Role of platelet-derived growth factors in angiogenesis and alveogenesis. *Curr Top Pathol* 93: 27–33, 1999.
32. **Liu T, Hu B, Choi YY, Chung M, Ullenbruch M, Yu H, Lowe JB, Phan SH.** Notch1 signaling in FIZZ1 induction of myofibroblast differentiation. *Am J Pathol* 174: 1745–1755, 2009.
33. **Mitchell KJ, Pinson KI, Kelly OG, Brennan J, Zupicich J, Scherz P, Leighton PA, Goodrich LV, Lu X, Avery BJ, Tate P, Dill K, Pangilinan E, Wakenight P, Tessier-Lavigne M, Skarnes WC.** Functional analysis of secreted and transmembrane proteins critical to mouse development. *Nat Genet* 28: 241–249, 2001.
34. **Morrow D, Scheller A, Birney YA, Sweeney C, Guha S, Cummins PM, Murphy R, Walls D, Redmond EM, Cahill PA.** Notch-mediated CBF-1/RBP-Jκ-dependent regulation of human vascular smooth muscle cell phenotype in vitro. *Am J Physiol Cell Physiol* 289: C1188–C1196, 2005.
35. **Nagy A.** Cre recombinase: the universal reagent for genome tailoring. *Genesis* 26: 99–109, 2000.
36. **Neptune ER, Podowski M, Calvi C, Cho JH, Garcia JG, Tuder R, Linnoila RI, Tsai MJ, Dietz HC.** Targeted disruption of NeuroD, a proneural basic helix-loop-helix factor, impairs distal lung formation and neuroendocrine morphology in the neonatal lung. *J Biol Chem* 283: 21160–21169, 2008.
37. **Nikolaou N, Watanabe-Asaka T, Gerety S, Distel M, Koster RW, Wilkinson DG.** Lunatic fringe promotes the lateral inhibition of neurogenesis. *Development* 136: 2523–2533, 2009.
38. **Noseda M, Fu Y, Niessen K, Wong F, Chang L, McLean G, Karsan A.** Smooth muscle alpha-actin is a direct target of Notch/CSL. *Circ Res* 98: 1468–1470, 2006.
39. **Ono Y, Sensui H, Okutsu S, Nagatomi R.** Notch2 negatively regulates myofibroblastic differentiation of myoblasts. *J Cell Physiol* 210: 358–369, 2007.
40. **Osada H, Tomida S, Yatabe Y, Tatematsu Y, Takeuchi T, Murakami H, Kondo Y, Sekido Y, Takahashi T.** Roles of achaete-scute homologue 1 in DKK1 and E-cadherin repression and neuroendocrine differentiation in lung cancer. *Cancer Res* 68: 1647–1655, 2008.
41. **Perl AK, Wert SE, Nagy A, Lobe CG, Whitsett JA.** Early restriction of peripheral and proximal cell lineages during formation of the lung. *Proc Natl Acad Sci USA* 99: 10482–10487, 2002.
42. **Post LC, Ternet M, Hogan BL.** Notch/Delta expression in the developing mouse lung. *Mech Dev* 98: 95–98, 2000.
43. **Powell DW, Mifflin RC, Valentich JD, Crowe SE, Saada JI, West AB.** Myofibroblasts. I. Paracrine cells important in health and disease. *Am J Physiol Cell Physiol* 277: C1–C9, 1999.
44. **Prodhan P, Kinane TB.** Developmental paradigms in terminal lung development. *Bioessays* 24: 1052–1059, 2002.
45. **Proweller A, Pear WS, Parmacek MS.** Notch signaling represses myocardin-induced smooth muscle cell differentiation. *J Biol Chem* 280: 8994–9004, 2005.
46. **Shan L, Aster JC, Sklar J, Sunday ME.** Notch-1 regulates pulmonary neuroendocrine cell differentiation in cell lines and in transgenic mice. *Am J Physiol Lung Cell Mol Physiol* 292: L500–L509, 2007.
47. **Shifley ET, Vanhorn KM, Perez-Balaguer A, Franklin JD, Weinstein M, Cole SE.** Oscillatory lunatic fringe activity is crucial for segmentation of the anterior but not posterior skeleton. *Development* 135: 899–908, 2008.
48. **Taichman DB, Loomes KM, Schachtner SK, Guttentag S, Vu C, Williams P, Oakey RJ, Baldwin HS.** Notch1 and Jagged1 expression by the developing pulmonary vasculature. *Dev Dyn* 225: 166–175, 2002.
49. **Tan JB, Visan I, Yuan JS, Guidos CJ.** Requirement for Notch1 signals at sequential early stages of intrathymic T cell development. *Nat Immunol* 6: 671–679, 2005.
50. **Tan JB, Xu K, Cretegny K, Visan I, Yuan JS, Egan SE, Guidos CJ.** Lunatic and manic fringe cooperatively enhance marginal zone B cell precursor competition for delta-like 1 in splenic endothelial niches. *Immunity* 30: 254–263, 2009.
51. **Tanigaki K, Han H, Yamamoto N, Tashiro K, Ikegawa M, Kuroda K, Suzuki A, Nakano T, Honjo T.** Notch-RBP-J signaling is involved in cell fate determination of marginal zone B cells. *Nat Immunol* 3: 443–450, 2002.
52. **Tsao PN, Chen F, Izvolsky KI, Walker J, Kukuruzinska MA, Lu J, Cardoso WV.** Gamma-secretase activation of notch signaling regulates the balance of proximal and distal fates in progenitor cells of the developing lung. *J Biol Chem* 283: 29532–29544, 2008.
53. **Tsao PN, Vasconcelos M, Izvolsky KI, Qian J, Lu J, Cardoso WV.** Notch signaling controls the balance of ciliated and secretory cell fates in developing airways. *Development* 136: 2297–2307, 2009.
54. **van Tuyl M, Groenman F, Kuliszewski M, Ridsdale R, Wang J, Tibboel D, Post M.** Overexpression of lunatic fringe does not affect epithelial cell differentiation in the developing mouse lung. *Am J Physiol Lung Cell Mol Physiol* 288: L672–L682, 2005.
55. **Visan I, Tan JB, Yuan JS, Harper JA, Koch U, Guidos CJ.** Regulation of T lymphopoiesis by Notch1 and Lunatic fringe-mediated competition for intrathymic niches. *Nat Immunol* 7: 634–643, 2006.
56. **Zhang N, Gridley T.** Defects in somite formation in lunatic fringe-deficient mice. *Nature* 394: 374–377, 1998.